Icarus **148**, 572–586 (2000)
doi:10.1006/icar.2000.6487, available online at http://www.idealibrary.com on IDEAL®

In-Flight Calibration of the Near Earth Asteroid Rendezvous Laser Rangefinder

Andrew F. Cheng and Timothy D. Cole

The Johns Hopkins University Applied Physics Laboratory, Laurel, Maryland 20723
E-mail: andrew.cheng@jhuapl.edu

Maria T. Zuber

Massachusetts Institute of Technology , 54-518, Cambridge, Massachusetts 02139, and NASA Goddard Space Flight Center, Code 920, Greenbelt, Maryland 20771

David E. Smith

NASA Goddard Space Flight Center, Code 920, Greenbelt, Maryland 20771

Yanping Guo

The Johns Hopkins University Applied Physics Laboratory, Laurel, Maryland 20723

and

Frederic Davidson

The Johns Hopkins University, 3400 North Charles Street, Baltimore, Maryland 21218

Received November 24, 1999; revised June 6, 2000

The Near Earth Asteroid Rendezvous (NEAR) mission began a year-long rendezvous with 433 Eros on 14 February 2000. The NEAR Laser Rangefinder (NLR) will measure ranges from the spacecraft to the surface of Eros with a single shot accuracy of a few meters. The NLR topographic data, when combined with doppler tracking of the spacecraft, will enable determinations of the asteroid's shape, mass, and density and will contribute to understanding of its internal structure and collisional evolution. NLR is the first space-borne laser altimeter with an in-flight calibration capability, achieved by means of an optical fiber which directs a small portion of every outgoing laser pulse back to the receiver with a known, fixed time delay. Key results of groundbased and in-flight calibrations of NLR are presented for: in-flight measurement of receiver noise statistics, confirmation of instrument stability over the 4-year cruise to Eros, absolute calibration of range measurements for ideal targets (flat, uniform surfaces normal to the boresight), and a prediction of single-pulse detection probability and range errors in the presence of pulse dilation from nonideal target surfaces, based on a Webb's approximation model of receiver performance. We find that pulse dilation is the major source of uncertainty in the single-shot range measurements from NLR, and that this uncertainty is consistent with the 6-m range measurement requirement for NEAR.

Key Words: **asteroids**; **asteroids, Eros**; **Surfaces, asteroids.**

INTRODUCTION

The Near Earth Asteroid Rendezvous mission (NEAR) was launched on February 17, 1996, inaugurating the NASA Discovery Program of low-cost planetary missions. NEAR began a year-long, orbital study of the near-Earth asteroid 433 Eros on 14 February 2000. NEAR is a three-axis-stabilized spacecraft that carries a five-instrument scientific payload, composed of a multispectral imager (MSI), a near-infrared spectrometer (NIS), an X-ray/gamma-ray spectrometer (XRS/GRS), a laser rangefinder (NLR), and a magnetometer (MAG). The scientific background and expected results of planned investigations on NEAR, including a radio science investigation using the spacecraft coherent X-band telemetry system, are summarized in a special issue of the *Journal of Geophysical Research* (Acuna *et al.* 1997, Cheng *et al.* 1997, Trombka *et al.* 1997, Veverka *et al.* 1997a, Yeomans *et al.* 1997a, Zuber *et al.* 1997). The spacecraft has been renamed NEAR Shoemaker in honor of Eugene M. Shoemaker (1928-1997).

On June 27, 1997, NEAR performed a flyby of the C-type main belt asteroid 253 Mathilde. At least five craters were found at diameters of 19 to 33 km, comparable to the 26.5-km mean radius of Mathilde (Veverka *et al.* 1997b). The NEAR flyby yielded the first direct mass determination for an asteroid (Yeomans

0019-1035/00 $35.00

et al. 1997b). With the measured mass of 1.033×10^{17} kg and an estimated volume of 78,000 km^3, the density of Mathilde was inferred to be 1300 ± 200 kg m^{-3}. Comparison of this density with that of carbonaceous chondrites suggests a porosity of ~50% for Mathilde. Subsequently, NEAR flew by Earth again on January 23, 1998, and all instruments were operated successfully (Izenberg and Anderson 1998).

On December 20, 1998, NEAR was scheduled to begin its rendezvous with 433 Eros, but the first rendezvous burn was aborted, and contact with the spacecraft was lost for 27 h. After recovery of communications, NEAR executed a flyby of Eros on December 23, 1998. The rendezvous burn was executed successfully on January 3, 1999. Results of the Eros flyby included determinations of the Eros mass $(7.2 \pm 1.8) \times 10^{15}$ kg and density (2500 ± 800) kg m^{-3} (Yeomans *et al.* 1999, Veverka *et al.* 1999). The size and rotation pole of Eros were found to be consistent with previous groundbased determinations (e.g., Yeomans, 1995).

During the rendezvous year at Eros, the NEAR Laser Rangefinder (NLR) will measure ranges to the surface with a single-shot accuracy <6 m at 50 km range (Zuber *et al.* 1997, Cole *et al.* 1997). NLR will produce high-resolution and high-accuracy topographic grids and profiles to determine the global shape, mass, and density as well as to characterize local and regional scale topography. These data will contribute substantially to understanding the internal structure, evolution, and collisional history of Eros. NLR will use the body-fixed, planetocentric longitude–latitude reference system derived primarily from images to produce the global topographic grid. Zuber *et al.* (1997) estimate that the mass of Eros will be determined to within 0.0001%, while the density will be determined to within 0.1%. Principal NLR data products will include a global topographic grid at ~500 m resolution and ~10 m radial accuracy, plus regional scale topographic models with ~5 m accuracy. In addition, joint observations of selected surface features are planned with MSI/NIS so that images and spectral data can be overlaid on topographic data.

The present work presents a complete description of NLR instrument operation and in-flight calibrations, including new information needed to analyze and interpret NLR range data. NLR differs from previous laser altimeters in that in-flight calibration is possible even without any target surface: an optical fiber is used to carry a portion of every emitted laser pulse back to the receiver with a known time delay. Also included here is a new model of the range uncertainties or "range walk" caused by pulse dilation, the temporal stretching of backscattered pulses due to surface tilt and roughness. This pulse dilation model is fitted to in-flight calibration data and yields predictions of NLR ranging performance at Eros. A full description of NLR instrument hardware, ground test, and prelaunch calibrations was given by Cole *et al.* (1997). Some calibration results presented below supercede those given earlier. An instrument software change will occur in June 2000 and will affect Eros data formats; unless noted otherwise, all information in this paper applies both before and after the software change.

NLR INSTRUMENT

NLR is a direct-detection, time-of-flight laser altimeter that determines the range from the NEAR spacecraft to the surface of Eros by measuring the round-trip travel time of laser pulses with 0.312 m range resolution (single count). It employs direct, incoherent detection using an all solid-state, diode-pumped laser transmitter, a Cassegrain receiver telescope, and a receiver electronics package that incorporates an IR-enhanced, silicon Avalanche Photo Diode (APD) with thresholding and timing electronics. Figure 1 shows the NLR flight hardware.

NLR is the first laser altimeter to employ continuous, in-flight calibration using a fiber-optic delay assembly (FODA), which is a spooled 109.5-m fused silica fiber-optic cable. Part of each optical pulse formed within the laser resonator is injected into the FODA, which injects a delayed optical signal directly into the receiver. This allows end-to-end calibration for each emitted pulse even when no target surface is available.

NLR is a bistatic system, with the transmitter separate from the receiver. The laser transmitter uses a diode-pumped, solid-state Cr:Nd:YAG with an active lithium niobate Q-switch to control the formation of the laser pulse. Similar lasers were used in the Clementine (Zuber *et al.* 1994) and Mars Global Surveyor (Zuber *et al.* 1992, Smith *et al.* 1999) laser altimeters. The transmission of the laser optical pulse is accomplished using a 62-mm Galilean refractive telescope, whose large aperture reduces beam divergence to 235 μr. The laser pulse repetition rate (PRF) can be selected from among $\frac{1}{8}$, 1, 2, and 8 Hz.

The receiver uses an 8.89-cm-diameter, gold-coated aluminum Dall-Kirkham telescope to focus backscattered laser energy onto the APD detector. The APD is a temperature-compensated, trans-impedance detector. Detected signals from the APD are amplified, passed through a 30-MHz Bessel filter, and sent to the time-of-flight (TOF) measurement system. The TOF system measures times from laser firing, as indicated by the laser transmitter start pulse, to the first receiver stop pulse (from the FODA calibration signal) and to the second stop pulse produced from the backscattered laser light returning from the target. The Bessel filter integrates the analog pulses to maximize the probability of detection for returned pulses that have been stretched in time ("dilated") by scattering from the rough, tilted target surface. The filter also attenuates high-frequency electronic noise. A comparator in the TOF system tests whether the filtered analog signal exceeds a commandable threshold voltage; when this occurs, a digital stop pulse is generated. The threshold level used by the comparator is set by ground command or autonomously through an auto-acquisition sequence. After the two TOF counters are stopped, a digital processing unit (DPU) reads the range measurements and formats them into science data packets together with instrument status and housekeeping information.

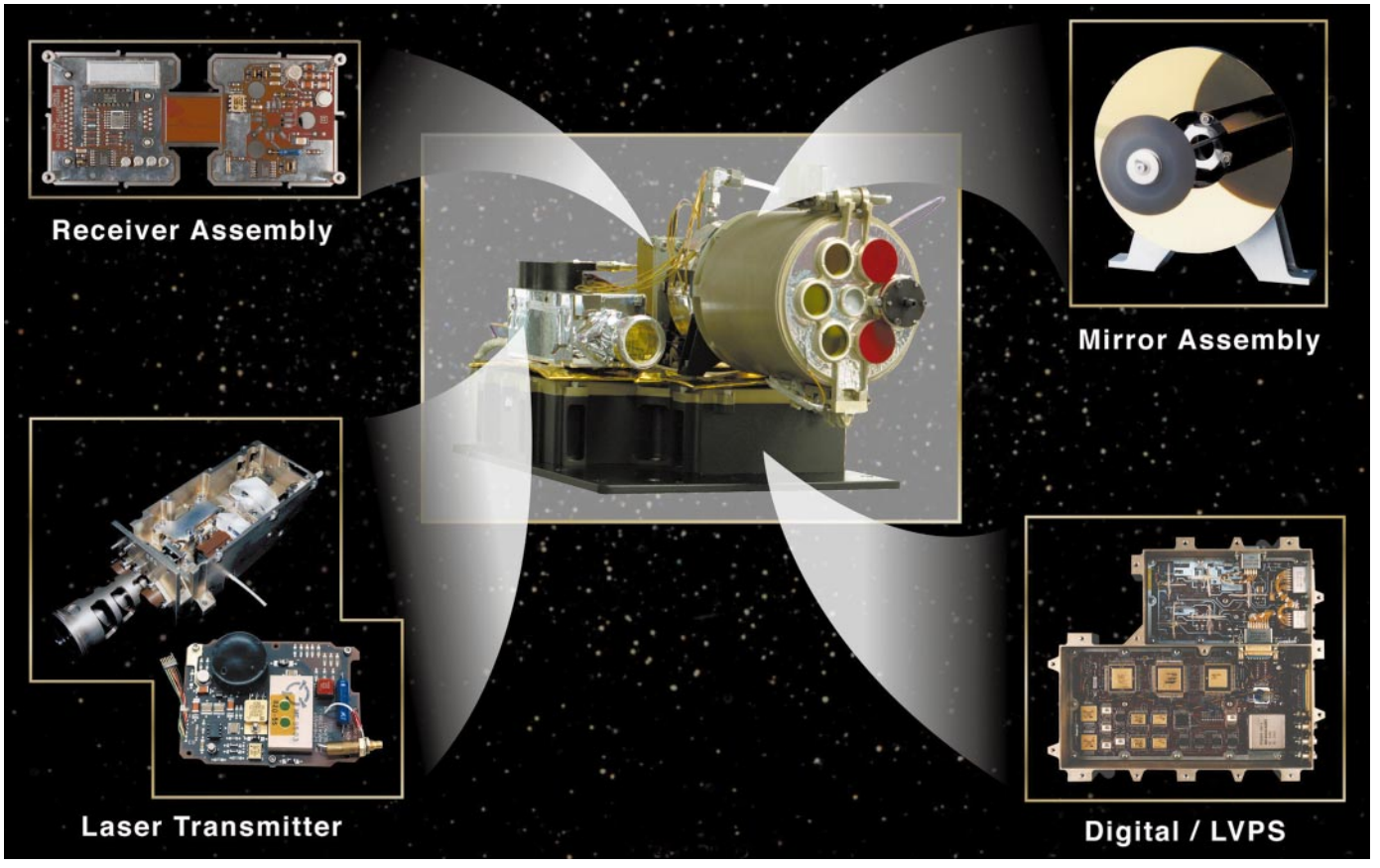

FIG. 1. NLR flight hardware.

OPERATION OF NLR

Measured laser pulse characteristics are summarized in Table I (data from Cole *et al.* 1997). The temporal, spatial (near- and far-field), and pulse energy characteristics were measured during NLR flight system development. Pulse energy measurements of the transmitter beam and FODA port output were measured using NIST-traceable equipment accurate to ±5%. Measured near-field spatial beam distributions included beam diameter ($1/e^2$), modal structure, and energy distribution characteristics. Far-field measurements included beam divergence, jitter, and wander.

The receiver sees two optical pulses per transmitted pulse. The first arrives ∼558 ns after laser firing and is the calibration pulse routed through the FODA. Detection of this pulse stops the calibration counter, yielding the calibration value ("Calibration" in Table AI; see Appendix). The next detected return is the surface backscattered pulse, stopping the range counter and yielding the range value ("Range" in Table AI).

NLR's receiver is a leading-edge detector, meaning that a stop pulse is generated as soon as the optically produced signal (the filtered, analog voltage from the calibration pulse or the target return) exceeds a threshold ("Threshold Voltage" in Table AI). The time when this signal crosses the threshold determines the measured TOF, which therefore depends on the threshold value, creating threshold-driven "range walk." This threshold can be commanded to any of eight values (Table I), although no calibration signal is detected at the highest value.

Figure 2 shows the sequence of events that occur with each laser shot. After the fire command, the laser pulse is generated after a time delay that varies from 170 to 190 μs. The firing time delay varies slowly on 10-min time scales. The emitted optical pulse generates the start pulse for the two TOF counters. The calibration pulse is received about 0.558 μs after firing, and the laser return from the target is received much later, at a time determined by the range (the range counter overflows after 2.18 ms). The NLR receiver is "blanked," or prevented from

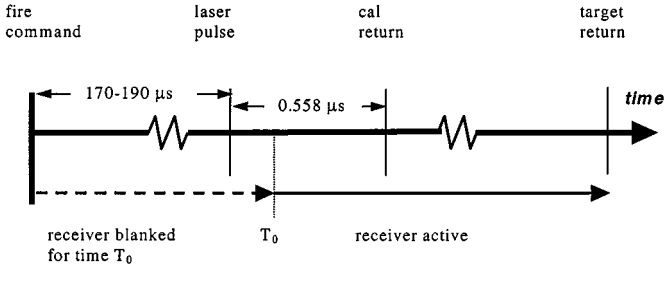

FIG. 2. Timing of instrument operation.

TABLE I
NLR Characteristics

Parameter	Measurement
Max. range (altitude)	327 km
Range accuracy	<6 m
Range precision	0.312 m
Pulse energy	15.3 mJ at 1.064 μm
Energy jitter	<1% rms knowledge
Pulse width	15 ns
Pulse width jitter	0.82 ns rms knowledge
Wavelength spread	$\pm$1 nm
Pulse frequency	1/8, 1, 2, 8 Hz
T-0 mask	0 to 511.5 μs, $\Delta = 500$ ns
Range gate	81 ns to 42.7 μs, $\Delta = 41.7$ ns
TEM_{00} (% Gaussian fit)	91% (TEM_{00} mode-like)
Divergence ($1/e^2$-points)	235 μrad
Calibration power jitter	$\pm$5%
Calibration timing jitter	<1.05 ns
Thermal control	<$\pm$2°C
Shots (lifetime)	$\sim 10^9$
Effective RX aperture, $f/\#$	7.62 cm, $f/3.4$
Spectral receiver Bandwidth	<7 nm
Temporal receiver Bandwidth	30 MHz
APD dark noise voltage	150 μV rms
APD hybrid responsivity	770 kV/W
Optical receiver FOV	2900 μrad
Threshold levels	16 mV $\times 2^n$, for $n = 0, 1, \ldots, 7$
Data rates	51 and 6.4 bps
Boresight shift, TX-to-RX	345 μrad

detecting a pulse, for a time interval T_0 after the fire command. This T-0 mask (see Table I) is set by ground command with a default value of 180.498 μs. In-flight tests have shown that this default value, as well as values half as large, are sufficient to prevent electronic noise from interfering with the receiver.

The value of T_0 is adjusted by two parameters returned in the NLR data; the first is called "T-0 COUNT" and is represented here by the symbol δ, while the second is called "Range gate" and is represented by the symbol r_g. This range gate parameter does not define a range gate in the usual sense of a brief time interval, during which the receiver is active, encompassing the time of the expected range return. Rather, the NLR receiver becomes active once the time T_0 has elapsed, and it remains active until two stop pulses are generated, one from the calibration return and one from the target. The relation between T_0 and the commandable parameters δ and r_g is

$$T_0 = 0.081 + r_g \times 0.0417 + \delta \times 0.5, \qquad (1)$$

where T_0 is in units of microseconds and where δ and r_g are both integers in the range [0, 1023].

The NLR timing shown in Fig. 2 applies to normal operation at any of the four PRF values. NLR also includes two special failure modes of operation, which can be used in the event of failures involving either the start pulse or the calibration pulse. In the former case, the FAILSAFE mode starts the TOF counters at the final value of the T-0 COUNT countdown. In the latter case, the ONESTOP mode causes NLR to use the first received stop pulse as the range pulse from the target. As of June, 2000, the start and calibration pulses are functioning nominally, and there is no plan to use either FAILSAFE or ONESTOP.

NLR has two additional special operating modes designed to enable autonomous operation without excessive ground commanding. The first is called "AUTO ACQUIRE," in which NLR uses the calibration pulse to find a threshold voltage above the noise level in the receiver. NLR fires 16-shot bursts at each of the eight possible values for the voltage threshold that are listed in Table I, which are labeled TH = 0 (for $n = 0$ in Table I) through TH = 7 (for $n = 7$). The results of all prelaunch and in-flight tests through May 2000 have shown that AUTO ACQUIRE sets the threshold at TH = 3. The second special operating mode is called "CALIBRATE," in which NLR autonomously sets the value of δ. During CALIBRATE, NLR increments δ until it finds as large a value as possible that still assures detection of a valid calibration pulse. Figure 2 shows that if δ becomes too large, the time T_0 that the receiver is blanked will include the arrival time of the calibration pulse, which cannot then be detected. As of May 2000 there is no plan to use CALIBRATE during asteroid operations because the default values of δ and r_g are completely satisfactory.

The timing of NLR events relative to other NEAR spacecraft events is shown in Fig. 3. All spacecraft events are coordinated by synchronization pulses sent over the Mil-Std-1553 data bus at each 1-s interval of mission elapsed time (MET) under control of the command and telemetry processor (CTP). These 1-s intervals are referred to as "major frames." Every major frame is divided into eight minor frames (Fig. 3) numbered 0 through 7, each lasting 125 ms. The NLR DPU controls instrument timing, which is locked to the receipt of the MET synchronization pulses once per second from the CTP. NLR fires the laser in specific minor frames, depending on the PRF mode as shown in Table II. In all cases, laser firing occurs within $\sim$3 ms of the start of the minor frame(s) shown in Table II.

Table II indicates that the laser firing times depend on the instrument software version number. Software Version 6 was used exclusively from launch through June 2000, when it will be replaced by Version 7. The laser firing times in 2-Hz mode will be changed in Version 7 to minor frames 2 and 6, instead

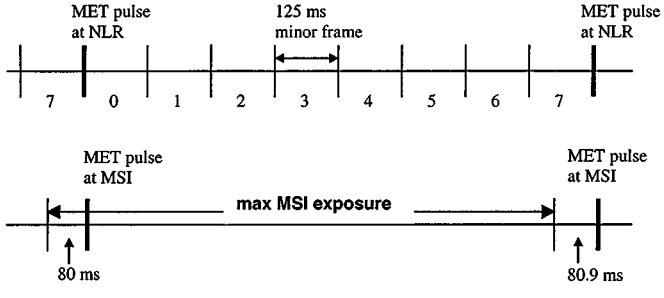

FIG. 3. Timing of NLR minor frames and MSI image exposures.

TABLE II
NLR Firing Times

PRF mode (Hz)	Minor frame (s)
$\frac{1}{8}$	4
1	4
2	0, 4, Version 6 2, 6, Version 7
8	All

of 0 and 4, to correct a spacecraft interface problem that gives a false overcurrent indication, causing NLR to be powered off. With the Version 6 software, NLR is shut off by the spacecraft within 3 s of operation at 2 Hz, unless the overcurrent protection is disabled. The 2-Hz mode will not be used to acquire data at Eros until this problem is corrected with the Version 7 software. The 2-Hz mode is needed to obtain contiguous samples while nadir pointed in 35-km orbit.

NLR can sustain continuous firing at $\frac{1}{8}$, 1, or 2 Hz PRF for indefinite periods. However, because of thermal limitation NLR cannot fire indefinitely at 8 Hz. In the 8-Hz mode, NLR fires 16 shots in 2 s, after which NLR is quiescent for 14 s. Hence, in this mode NLR fires an average of one pulse per second.

An important NLR science objective is to correlate the laser altimetry data with imaging data from the NEAR Multispectral Imager (MSI), as discussed by Zuber *et al.* (1997). To accomplish this objective, it is necessary to determine the boresight offset between the NLR and the MSI. Both instruments have been designed to enable a direct measurement of the boresight offset, by using MSI to image the laser spot over the dark side of Eros. To obtain sufficient signal in the image, NLR is operated at 8 Hz to produce eight shots during the maximum imager exposure time of 999 ms. The relative timing of NLR operation and MSI image exposures is shown in Fig. 3. The MET synchronization pulses at NLR and at MSI are time-aligned within a few milliseconds. During the maximum MSI exposure, the first NLR shot occurs ~80 ms after the start of the exposure, and the last occurs ~44 ms before the end, provided that shots are fired in every minor frame. When operated in Version 7, NLR will always begin a 16-shot, 8-Hz burst in minor frame 0, so two full major frames will have shots in every minor frame. In Version 6, an 8-Hz burst can begin randomly in any minor frame.

NLR DATA COLLECTION

During Eros rendezvous, NLR will fire laser pulses whenever the instruments are pointed at Eros for data acquisition (all the instruments can observe Eros simultaneously). NEAR Shoemaker acquires data for approximately 16 h per day and downlinks data for approximately 8 h per day. During downlink periods, NLR will not be pointed at the asteroid but will remain powered on. If NLR is operated in the 1 Hz mode, it will obtain a total of $\sim 2 \times 10^7$ range measurements during the year-long prime mission and generate up to ~1.7 G bit of data. NLR commenced data acquisition at Eros when the spacecraft descended to within 300 km range from the surface of Eros on 28 February 2000.

During the first 2 weeks of May 2000, NLR controlled the spacecraft attitude while in an approximately circular, 50-km polar orbit (measured from the center of mass). Most of the NLR data will be acquired while nadir pointing, with NLR pointed to the Eros center of mass, or while pointed at a fixed angular offset from nadir. Figure 4 shows the ground coverage for 1 week of

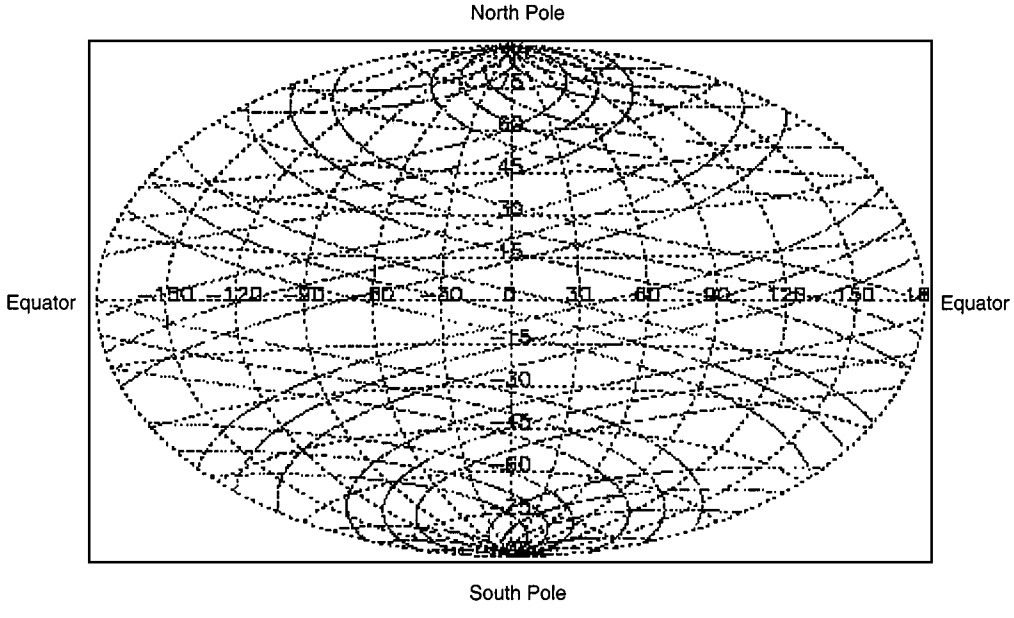

FIG. 4. Global coverage of Eros from one week of nadir-pointed observations in the 50 km circular, polar orbit. Sub-spacecraft tracks are shown on a longitude–latitude grid.

nadir-pointed observations in the 50-km polar orbit. The footprints of successive laser shots at 1 Hz PRF will be significantly overlapping while NLR is nadir-pointed during most of this orbit, except when NEAR is directly over an elongated end of Eros (Zuber *et al.* 1997, Cole *et al.* 1997). The footprint diameter is 7 m at an altitude of 30 km and at normal incidence. The sub-spacecraft point on Eros moves at 3–5 m/s. Even 1 week of nadir-pointed observations will yield a data set well suited for determining global shape, size, and rotation state (Zuber *et al.* 1997). Although each NLR track is densely sampled in the 50-km orbit, Fig. 4 shows that the successive tracks are spaced more than 1 km apart at the equator of Eros. Cross-track scanning of NLR, using spacecraft maneuvers, will be used to obtain a more uniform areal coverage of Eros.

Since the laser footprints are overlapping or nearly so at 1 Hz PRF while nadir-pointed in the 50-km orbit, NLR operations through June 2000 will use the 1-Hz mode. Once the spacecraft descends to 35 km orbit, the 1-Hz PRF will no longer suffice for contiguous samples, and NLR will be operated at 2 Hz using Version 7 software.

NLR DATA FORMATS

NEAR uses Consultative Committee for Space Data Systems-compliant data packet formats, of which two formats, normal and high rate, are used for NLR science data. With software Version 7, all data will be returned in the normal format. With Version 6, the normal format is used for $\frac{1}{8}$-, 1-, and 8-Hz PRF data, whereas the high-rate format is used only for 2-Hz data. Cruise phase calibration data in the 2-Hz mode were returned in the Version 6 high-rate format, but no Eros data. All Eros data are in the normal format.

Both data formats have a packet length of 2864 bits and are constructed as follows: primary header (48 bit), secondary header (48 bit), user data, and instrument status (2768 bit). The normal NLR data format has user data for 56 shots and 80-bit instrument status. The high-rate format has user data for 112 shots and 80-bit instrument status. The status bits are the same for the two data formats. Several data values present in the normal format for each shot are not included in the high-rate packet format, because each high rate packet includes 112 shots, whereas only 56 shots are included in a normal format packet of the same length.

The spacecraft packet telemetry stream consists not only of NLR packets but also those from other instruments and spacecraft housekeeping. The NEAR Science Data Center (SDC) processes the packet data to generate NLR Experiment Data Records (EDRs) containing the information needed for NLR data analysis (Cheng *et al.* 1997, Heeres *et al.* 1997). The NLR EDRs take the form of Flexible Image Transport Standard (FITS) files, in which each packet makes up one record. The NLR FITS files are organized such that all the normal format packets from any UTC day are compiled into one file, while all the high-rate packets from the same day are compiled into another file. The FITS file naming convention is as follows: for the normal format FITS file, LyydddNT.FIT is used where L means laser, and yyddd represents digits giving date of observation in two-digit-year and day-of-year format; correspondingly, for the high-rate format FITS file LyydddHT.FIT is used. An example is L96116HT.FIT for data obtained at 2 Hz on April 25, 1996.

While the NLR packets contain basic information on the instrument status, additional information on the state of the instrument is returned in the spacecraft housekeeping packets. The SDC merges this additional information with that from the NLR packets to produce the NLR FITS files. A full listing of the data values in the NLR FITS files with complete definitions is given in the Appendix.

LABORATORY CALIBRATION OF RANGE MEASUREMENT

The absolute calibration of NLR range measurements, or the relation between measured TOF and range, was measured in laboratory tests prior to launch (Cole *et al.* 1997). Two separate measurements were obtained: first, a determination of the total system delay in commanded threshold TH = 2, and second, a determination of how this delay varies with TH (threshold-based range walk). The total system delay is the time between the arrival of a laser pulse and the electronic registration of counts, and it was determined by comparing the time delay of an optical pulse through the FODA in two cases: FODA separate from the NLR (529.2 ns delay), and FODA integrated with the NLR receiver at commanded threshold TH = 2 (558.33 ns delay). The total system delay T_{sd} was measured as the increase in the time delay when connected to NLR, or 29.13 ns.

This measurement was confirmed, and the threshold-based range walk was measured, during the absolute calibration tests performed on August 8–9, 1995 ("hall shot test," Zuber *et al.* 1997). The completed instrument was used just prior to integration with the spacecraft, ranging to a sand-blasted aluminum target at a range of 182.88 m measured with an NIST-traceable surveyor's rule. NLR was fired in TH = 4 at 1 Hz PRF with the window cover closed and with neutral density filters to achieve a total of 71 db optical attenuation. The measured range was 601 counts. From the NLR oscillator speed of 480 MHz $\pm$ 0.0005% (correcting the drift specification given by Cole *et al.* 1997), each count equals 2.0833 ns in time-of-flight. Hence the uncorrected one-way range was measured as 187.68 m, exceeding the true range by 4.80 m. The excess range converts to an excess of 32.0 ns in the measured time-of-flight caused by the combination of total system delay and the threshold-based delay (at a higher detector threshold, the count is registered at a later time, when the received signal exceeds the threshold; this "range walk" delay depends on the pulse shape). Based on data from Fig. 18 of Cole *et al.* (1997), the threshold-based range walk delay from TH = 2 to TH = 4 is 2 counts, or 4.16 ns. The sum of total system delay (measured above as 29.13 ns) and range walk delay is 32.3 ns, which agrees well with the direct measurement of 32 ns excess time-of-flight. We conclude that the total system delay is

29 ns, with a (conservative) uncertainty corresponding to half a count, which is 1 ns or 15.6 cm in range.

We note that the prelaunch data in Fig. 18 of Cole *et al.* (1997) and in Fig. 7 of Zuber *et al.* (1997) showing calibration counts versus TH are superceded by the in-flight calibration data presented in this paper. This is because the FODA used for the August 1995 hall shot test was damaged during later ground handling and was replaced by the flight spare unit prior to launch. Hence the cited prelaunch data do not apply to the flight instrument, whose calibration counts versus TH characteristics are slightly different, as shown below. However, the measured total system delay of 29 ± 1 ns, as measured in August 1995, does apply to the NLR as flown, because the total system delay is caused by propagation in the instrument optics and by electronic delays, both of which are not affected by replacement of the FODA.

IN-FLIGHT CALIBRATION RESULTS

A summary of all in-flight tests of NLR through the end of November 1999 is given in Table III. These include functional tests in addition to those intended for calibration. The Earth swingby test involved attempts to use NLR to illuminate a receiver at the NASA Goddard Space Flight Center and to detect laser pulses transmitted from the same site. Owing to cloudy sky conditions throughout the scheduled test, results were inconclusive (Izenberg and Anderson 1998). The SEQGEN test involved commanding NLR via SEQGEN, a scheduling tool developed by the Jet Propulsion Laboratory that is used for Eros operations.

An extensive series of in-flight calibration tests was performed to measure the calibration counts versus TH characteristic of the flight FODA and to monitor this characteristic for changes over the 4-year cruise to Eros. Figure 5 plots the calibration counts versus commanded threshold TH for all in-flight tests through August 1999. The calibration count values have been stable within ~0.5 count since launch, and the 1999 test results (displaced downward by 2 counts in Fig. 5) are even more tightly clustered. An increase in the slope of the curve from TH = 5 to TH = 6 is evident for each of the observation dates. The same increase in slope above TH = 5 can be seen in Fig. 7a of Zuber *et al.* (1997) obtained from the hall shot test FODA that was not flown. The slopes of the calibration count vs TH curves are diagnostic of the laser pulse shape relative to the threshold voltage levels (that is, the slope measures the time in counts for the signal to rise 3 db, the interval from one threshold to the next). The increase in slope above TH = 5 indicates that the comparator voltage level in TH = 6 is already approaching the maximum signal level in the received calibration pulse. This suggests that the calibration pulses are not seen for the next higher threshold TH = 7 because the received calibration signal never exceeds the TH = 7 threshold, which is 3 db higher than that in TH = 6.

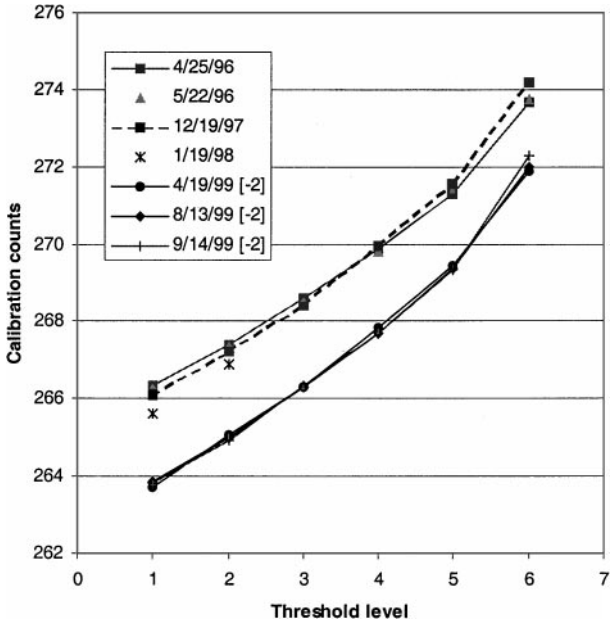

FIG. 5. Calibration counts versus threshold setting measured in-flight. Data from 1999 tests have been offset downward by 2 counts for clarity.

The measurements of total system delay and threshold-based range walk yield the conversion from range counts to range R in meters measured by NLR,

$$R = 0.3122838 \times \text{counts} - \text{corr(TH)} - 4.37, \qquad (2)$$

TABLE III
NLR In-Flight Calibration Tests through November 1999

Observation	Date	DOY	Start UTC	End UTC	Duration (s)	MET start	MET end
Calibration and test	4/25/96	116	7:07:47	22:44:16	56189	5826259	5882448
Calibration and test	5/22/96	143	21:07:45	21:46:49	2344	8209458	8211802
Calibration and test	9/24/97	267	20:40:58	21:25:38	2680	50543860	50546540
Calibration and test	12/19/97	353	15:15:38	19:29:24	15226	57954741	57969967
Earth swingby	1/19/98	19	0:54:55	6:43:19	20904	60581499	60602403
Calibration and test	4/19/99	109	15:07:44	20:10:41	18177	99944681	99962858
SEQGEN test	8/13/99	225	12:00:04	14:41:12	9668	109955824	109965492
MSI-NLR align	9/14/99	257	20:40:04	23:41:39	10895	112751825	112762720

TABLE IV
Range Corrections in Meters vs TH

TH	corr (TH), 4/99 and 8/99	corr (TH), previous tests
1	−0.37	−0.36
2	0	0
3	0.40	0.51
4	0.84	0.92
5	1.38	1.38
6	2.17	2.15

where the last term accounts for the total system delay of 29 ns and where the correction corr(TH) is listed in Table IV and accounts for the threshold-based range walk.

The threshold-based range walk corrections in Table IV were obtained from in-flight calibration tests. The calibration counts for all shots with a given TH are averaged from a given test, omitting shots without valid calibrations (e.g., FAILSAFE data, also data with range gate values that suppress the calibration pulse). Each entry in Table IV is the average of >1000 valid calibrations. The difference in average calibration counts between the given threshold and TH = 2 yields the range correction in Table IV, using the conversion 0.3122838 m per count. The TH = 2 correction is zero by definition. No calibration pulses are detected for TH = 7 so no range correction is shown, and none is shown for TH = 0, which is at the noise level and which will not be used for mapping.

The second column of Table IV shows the threshold-based range walk corrections from the combined data sets obtained in the flight tests performed 4/19/99 and 8/13/99. The values in the second column will be adopted for initial analyses. The third column shows, for comparison, the corrections obtained from the combined data sets obtained in all flight tests from launch through 1998. The changes in these corrections over the >3-year time span are regarded as a conservative estimate of the uncertainties in the corrections. The uncertainty in corr(TH) corresponds to less than 11 cm range.

We now estimate the single-shot range uncertainty when ranging to an ideal target (a flat, diffusely reflecting surface normal to the boresight). The contributions to this range uncertainty as discussed above are collected in Table V. The entry under "range counts" is ±0.5 count in the measured TOF. The uncertainties are statistically independent and are combined by the square root of the sum of the squares (rss). The uncertainty due to oscillator drift is ±0.0005% of the measured range, based on prelaunch tests. The actual oscillator drift after 4 years in space can be estimated from analysis of range measurements to Eros obtained from different orbit altitudes. As NEAR descends to progressively lower orbits, the measured ranges should decrease accordingly; this allows estimation of the oscillator drift from the data. The orbit can be determined independently of NLR from radio tracking and optical navigation.

TABLE V
Single Shot Range Uncertainty, Ideal Target

Contribution to uncertainty, single shot	Range uncertainty (m)
Range counts	±0.156
Threshold-based range walk	±0.11
Total system delay	±0.156
Oscillator drift, ±5 ppm	±0.2 at 40 km range
Total (rss)	±0.32 (at 40 km)

Finally, Table V does not include the effect of pulse dilation caused by reflection from a nonideal target surface, which may dominate the single-shot ranging uncertainty at Eros. In addition, no temperature corrections to measured ranges are needed. In-flight tests have confirmed that any temperature-induced range errors are negligible on NLR (see Appendix). We note that calibration errors have been estimated on a best-effort basis, but measurement errors will be slightly greater.

MODEL OF RECEIVER PERFORMANCE WITH PULSE DILATION

The probability of successful ranging measurement (P_d) depends on the surface reflectivity of the target, distance from the target, surface height distribution within the laser footprint, target surface tilt, transmitted laser pulse energy, receiver telescope aperture, and the noise levels within the receiver. A simple receiver model is presented below that predicts the NLR single-shot detection probability using Webb's approximation (Gardner 1992, Cole *et al.* 1997). The new result here is that the NLR FODA enables for the first time an in-flight measurement of the key receiver parameter that determines the single shot detection probability at a given threshold setting, namely, the ratio of threshold voltage to receiver noise. The main idea is that the model predicts not only the probability of detecting the reflected signal pulse, but also the probability of false alarm, which is the probability that receiver noise will exceed the threshold and generate a false TOF. The false alarm rates have been measured in-flight at NLR's lowest two threshold levels that are within or close to the receiver noise level. With the aid of the Webb's approximation receiver model, these in-flight calibrations yield determinations of the receiver noise and lead to predicted probabilities of successful ranging by NLR.

The NLR receiver model, as calibrated by in-flight tests, is also combined with a model of pulse dilation by a tilted target surface. Pulse dilation is the temporal stretching of a returned pulse when compared to the transmitted pulse and comes about when different parts of the laser-illuminated target area are at different ranges from the instrument, so measured TOF values are dispersed. The pulse dilation model outlined below predicts the return pulse intensity versus time from a diffusely reflecting, planar target at nonnormal incidence. Surface roughness also contributes to pulse dilation (e.g., Gardner 1992), but the effects

TABLE VI
Radiometric Inputs

Input	Symbol	Value
Transmitted pulse energy (J)	E_t	15 e-3
APD quantum efficiency	η_{APD}	0.35
Photon energy (J)	$h\nu$	1.867 e-19
Collecting area (m^2)	A	0.00456
Range from target (m)	R	Input
Receiver transmission	η_{rcv}	0.8
Solar irradiance ($W/m^2/\mu$)	I_{solar}	Input
Reflectance of target	r_{diff}	0.2
Receiver bandpass (μ)	$\Delta\lambda$	0.007
Receiver field of view (rad)	θ_{fov}	0.0029

of surface roughness and tilt are not separable by a leading edge detection system such as used by NLR (characterization of the received pulse waveform would be needed to do so). Hence, the receiver model predicts NLR's single-shot probability of detection from a tilted target surface, and, at the same time it yields estimates of the range walk error induced by pulse dilation. In addition, comparison with measurements of Eros may yield constraints on the "effective" surface tilt within the laser footprint, where this effective tilt includes a contribution from surface roughness.

The key radiometric parameters of NLR are defined in Table VI, which also lists the adopted parameter values from Cole *et al.* (1997).

The number of signal photoelectrons generated per pulse is then

$$n_s = \frac{E_t}{h\nu}\frac{r_{diff}}{\pi}\frac{A}{R^2}\eta_{rcv}\eta_{APD}, \tag{3}$$

which evaluates to $n_s = 181$ photoelectrons per pulse at a range of 190 km, a typical altitude above the surface during NLR's initial mapping operations from 200 km circular orbit. In what follows, the rate at which reflected laser photons are absorbed per second is written ϕ, and the total number of photons absorbed per pulse is written $\phi\tau_p$, where τ_p is the (dilated) pulse width. The solar irradiance is 230 $W/m^2/\mu$ at 1.68 AU from the Sun, a typical value for the 50-km circular polar orbit at Eros, and the 1.064-μ Eros albedo is from groundbased observations (e.g., Murchie and Pieters 1996). The number of solar background photoelectrons per second is written ϕ_b,

$$\phi_b = \frac{\eta_{APD}}{h\nu} I_{solar}\Delta\lambda\eta_{rcv}\pi\left(\frac{\theta_{FOV}}{2}\right)^2\frac{r_{diff}}{\pi}A,$$

which evaluates to $\phi_b = 4.63e+09\ s^{-1}$ for the given inputs.

Pulse dilation from a nonideal target surface is simply modeled here by considering a planar target which is inclined to the boresight, although the model can be generalized to the case of a rough, nonplanar target surface. The transmitted pulse shape is assumed to be a Gaussian with mean = 19 ns and FWHM = 12 ns, but truncated to be zero for times $t < 0$ (the start time is $t = 0$) and $t > 39.6$ ns. The beam angular distribution is assumed to be Gaussian also with full width at e^{-2} of peak intensity at 235 μr. The target surface is assumed to be planar but tilted to the line of sight with specified incidence angle. It is a distance R from the instrument along the boresight direction (the center of the emitted beam). A uniform, rectangular grid is defined on the target plane, and the ranges from the instrument to each grid cell are denoted R_{ij}, $i = 1, \ldots, 20$ and $j = 1, \ldots, 20$. The returned photons from each grid cell arrive at a time

$$t_{arrival} = t_{transmit} + 2R_{ij}/c,$$

which is calculated for each transmit time and grid cell ij. The number of photons from each grid cell at $t_{arrival}$ is determined from the transmit time relative to the (truncated) Gaussian pulse shape and from the angular displacement of the grid cell off the boresight. Each grid cell is assumed to have the same reflectivity. The total number of received photons per pulse is normalized to n_s/η_{APD}. The transmit time is discretized in units of one receiver time-of-flight count, which is 2.083 ns. Finally, the numbers of photons from the various grid cells are sorted by arrival time to determine the returned number of photons from the entire target versus time.

The APD and receiver characteristics are modeled as in Cole *et al.* (1997) using Webb's approximation in which the statistical distribution of the number of photoelectrons approaches a Gaussian near the mean value $G\phi\tau_p$ with a variance $FG^2\phi\tau_p$, where the APD excess noise factor F is given by

$$F = k_{eff}G + (2 - 1/G)(1 - k_{eff})$$

and the APD parameters are given in Table VII. For NLR, the excess noise factor $F = 2.627$.

The effective signal pulse width τ is approximated as the greater of the receiver filter time constant τ_1 and the dilated pulse width (defined as time interval from receipt of 10 to 90% of total pulse energy, as computed above),

$$\tau = \max(\tau_1, \text{dilated pulse width}).$$

The mean APD outputs are μ_0 in the absence of signal and μ_1

TABLE VII
Receiver Parameters

Parameter	Symbol	Value
Receiver filter time (s)	τ_1	60 e-9
Surface leakage (A)	I_s	2.00 e-08
Bulk leakage current (A)	I_b	5.00 e-11
APD gain	G	100
Ionization coefficient ratio	k_{eff}	0.0065
Feedback resistor (ohm)	R_1	22000
Preamp noise temp (K)	T_n	750

with signal, where

$$\mu_0 = \left(\lambda_b X + \frac{I_b}{e} + \frac{I_s}{eG}\right)\tau$$
$$\mu_1 = \mu_0 + n_s X,$$

where

$$X = \frac{\tau_1}{\tau}.$$

Here e is the elementary charge. The variance of the preamplifier and APD leakage current noise σ^2 is given by (k is the Boltzmann constant)

$$\sigma = \left[\frac{2kT_n\tau}{R_1 e^2} + \frac{I_s\tau}{eG}\right]^{1/2}.$$

In the case of no signal, the APD output is described by the distribution function $P_{PD0}(z)$,

$$P_{PD0}(z) = \frac{1}{\sqrt{2\pi}}\frac{1}{\left[1+\frac{G(F-1)z}{s_{00}}\right]^{1.5}}\exp\left[\frac{-z^2}{2\left[1+\frac{G(F-1)z}{s_{00}}\right]}\right],$$

where $s_{00} = \sqrt{G^2 F \mu_0}$.

With signal present, the APD output is described by

$$P_{PD1}(z) = \frac{1}{\sqrt{2\pi}}\frac{1}{\left[1+\frac{G(F-1)z}{s_{11}}\right]^{1.5}}\exp\left[\frac{-z^2}{2\left[1+\frac{G(F-1)z}{s_{11}}\right]}\right]$$
$$s_{11} = \sqrt{G^2 F \mu_1}.$$

The probability of false alarm P_{FA} is then given by

$$P_{FA} = 1 - \exp\left[-\frac{T}{\tau}\int_{z_0}^{z_1} P_{PD0}\,\mathrm{erf}\left(\frac{s_{00}z - n_T s_0}{\sigma}\right)\mathrm{d}z\right] \quad (4)$$
$$s_0 = \sqrt{s_{00}^2 + \sigma^2},$$

where n_T is the threshold level normalized to the noise level, which is fitted to in-flight calibration data. Constant values of z_0 and z_1 are chosen to include the entire variation of the integrand. Here T is the time from laser firing to photon return, and P_{FA} is calculated as a function of T for a given value of n_T. The function erf(z) is the cumulative distribution function of a Gaussian random variable with zero mean and unit variance.

Similarly, the single shot probability of detection P_D is

$$P_D = \int_{z_2}^{z_3} P_{PD1}\,\mathrm{erf}\left(\frac{s_{11}z - n_T s_0 + G n_s}{\sigma}\right)\mathrm{d}z \quad (5)$$

and constant values of z_2 and z_3 are chosen to include the entire variation of integrand. Both integrals are evaluated by numerical quadrature.

PREDICTED RANGING PERFORMANCE AT EROS

The model outlined above is fitted to in-flight calibration data of NLR. There are three relevant observations. First, in TH = 0, the false alarm rate as measured on 4/19/99 was 62%, defined as the fraction of shots in which the range count was less than the correct value of 264 (this value is the correct calibration count, because the arrival of the calibration pulse also stops the range counter in TH = 0). The range count of 264 corresponds to a range window open to 82.4 m. Second, in TH = 1, the false alarm rate as measured on 4/19/99 was 45.6%, defined analogously as the fraction of shots in which the range count did not overflow (overflow occurs at a count of 1048450, so the range window was open to 327.4 km). Finally, in TH = 2 the false alarm rate was not measurable (no false alarms seen in 372 shots on 4/19/99 or in 5224 shots on 1/19/98).

The measurements are reproduced by the Webb's approximation model with inputs as listed above (except, of course, that there is no solar background), and with the fitted n_T values in Table VIII. The threshold voltage count values are returned in the NLR telemetry (see Appendix), so the ratio of the threshold voltages in TH = 1 versus TH = 0 is known independently from the NLR housekeeping data. The n_T values in Table VIII are consistent with these in-flight data. The P_{FA} value could not be measured for TH = 2, so the values given in Table VIII are the model predictions based upon an n_T value of 10 as inferred from the NLR housekeeping data.

These results are applied to ranging to the sunlit surface of Eros from the 200-km orbit (nominal range 190 km). The top panel of Fig. 6 shows the cumulative number of photons received (dashed curve) versus range from the tilted target surface at 20° incidence angle (boresight to surface normal). Although NLR will be nadir pointed, the asteroid is nonspherical, and incidence angles of 20° or larger are expected. The solid curve shows a single shot probability of detection approaching unity from the 200-km orbit. The mean value of the measured range, as estimated from the range at which the probability of detection reaches half of its ultimate value, is 190.0003 km, implying a range walk error of +0.3 m induced by pulse dilation. The probability of false alarm is predicted to be 0.04%, which is negligible.

The bottom panel of Fig. 6 shows the effect of pulse dilation at the same nominal range, but with a greater surface tilt. At 35° incidence, the total probability of detection decreases to 62%, and the range walk error is now +8 m. The false alarm

TABLE VIII
In-Flight Calibration of Receiver Noise

4/19/99	n_T	P_{FA}	$cT/2$
TH = 0	1.3	0.618	82.4 m
TH = 1	4.5	0.456	327.4 km
TH = 2	10	$\ll 10^{-4}$	327.4 km

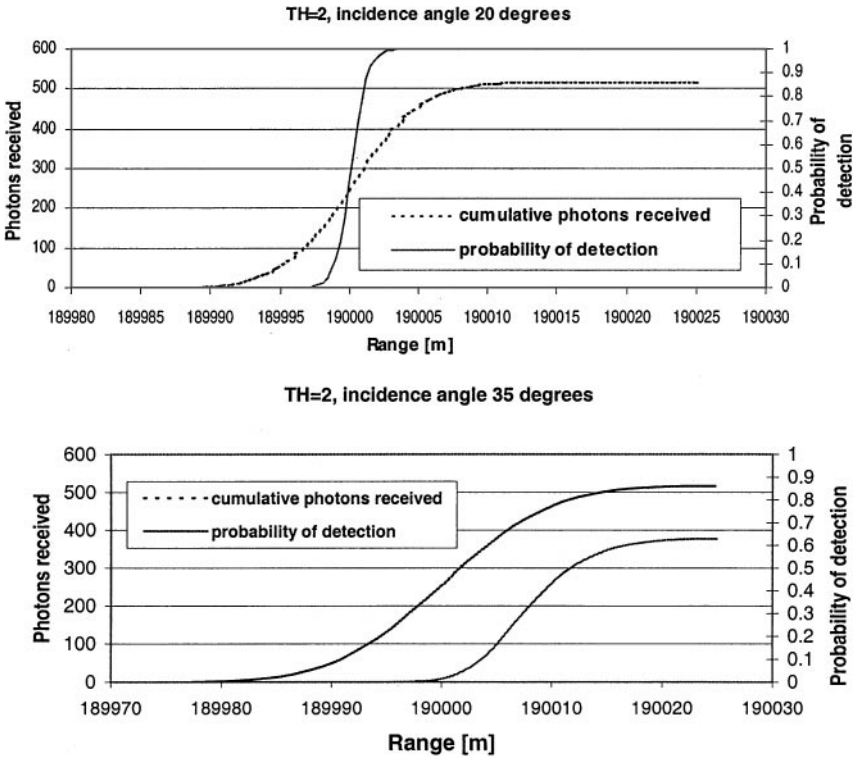

FIG. 6. Effect of pulse dilation on single shot detection probablity, ranging to dayside from 190 km altitude at 20° (top) and 35° (bottom) incidence angle.

probability becomes 0.7% which is acceptable. Hence, NLR is expected to range successfully to Eros from the 200-km orbit at up to ∼35° incidence. At shorter ranges, the number of returned signal photons is much greater and the pulse dilation is less, because of the smaller laser footprint. The probability of detection is higher, allowing operation at significantly off-nadir pointing and high incidence angle. For example, calculations show that in the 50-km polar orbit, with a nominal range of 40 km and an incidence angle of 45°, the probability of detection at TH = 6 is essentially unity and the range walk error from pulse dilation is −0.9 m. Ranging accuracy from 50 km orbit is fully consistent with the 6-m science requirement (Zuber *et al.* 1997).

NLR commenced science operations at Eros on February 28, 2000, when the first laser returns were detected at a range of 300 km. Science data acquisition has been accomplished successfully in orbits at 200, 100, and 50 km, qualitatively confirming the predictions of instrument performance from Webb's approximation. A quantitative comparison is difficult, because in the high orbits the incidence angles at the scale of the laser footprints are not well known, whereas in the low orbits P_d has been essentially unity. A detailed analysis of instrument performance at Eros will be presented elsewhere.

APPENDIX I—NLR DATA FORMATS

The NLR Experiment Data Records take the form of FITS files. These are the time-ordered, raw data products from the merging of NLR science data packets with instrument data extracted from spacecraft housekeeping packets. The two NLR packet formats, normal and high rate, are made into separate FITS files and are not merged with each other. As discussed in the text, NLR packets contain primary and secondary headers plus user data and status bits. Details are given in Table AI, which shows in the first column whether a data value is found in the headers, user data, or status bits. In both NLR packet formats, the primary header information is used for telemetry processing and is not pertinent to data analysis, while the secondary header contains the packet Mission Elapsed Time (MET, 32 bit), software version number, and subprocess identifier (normal or high rate). Not all of the user data values in the normal format are included in the high rate format, as shown in the second and third columns of Table AI. The software version number is 6 for all data from launch through June 2000, after which software version 7 will be used. All information in this Appendix applies to either Version 6 or Version 7 except where stated otherwise. The most significant differences between the data formats in Versions 6 and 7 are

- Version 7 returns all data in the normal format, including 2-Hz mode data;
- In Version 7, the first three fields in the science status bits are: Last Cal (calibration count of the last shot) and then the minor frames of the first shot and the second shot of the packet. These three fields replace the first two fields in the Version 6 normal format, which are Last Cal and First Cal.

As a general rule, data constants are converted to decimal integers in the NLR FITS files. For example, the 12 least significant bits of the 32-bit MET are returned for each shot in the normal format data (Table AI) and are converted to an integer in the range [0, 4095]. The "Range" counts are converted to integers [0, 1048580]. The conversion from "Range" counts to range is given in the text. The "Calibration" counts measure the time delay introduced by the FODA and are returned for each shot in the normal format; additionally, the same "Calibration" count values for the first shot and the last shot in the packet are returned among the status bits (version 6 only). In the high rate format, calibration counts are returned only for the first and last shots in the status bits.

The NLR FITS files contain 8640 bytes of header information, including lists of all data values in the NLR packets (Table AI) and all values from spacecraft housekeeping (Tables AIIa and AIIb). Following the header, packet data are

TABLE AI
NLR Science Packet Data

Location	Normal format	High rate format	Comment
Packet header	MET	MET	Mission elapsed time in seconds, 32 bits
	Software version	Software version = 6	Version 6 or 7
	Subprocess ID = 4	Subprocess ID = 5	
User data, each shot	56 Shots included	112 Shots included	
	MET	(not included)	12 Least significant bits of MET
	Range	Range	Max = 1048580
	Threshold	(not included)	Commanded threshold 0, 1, . . . , 7
	Calibration	(not included)	Counts
	TxReady	TxReady	If transmitter is ready to fire, TxReady = 0
	NoReturn	NoReturn	If range overflow, NoReturn = 1
Status bits			
	Last Cal	Last Cal	Counts, last shot
	Status 2	First Cal	See Table AIa
	Spare	Spare	Always equals zero
	T-0 count	T-0 Count	Adjusts T-0 mask
	Last command	Last command	Op-code, decimal; see Table AIII
	Threshold voltage	Threshold voltage	Counts
	Time-of-flight temp	Time-of-flight temp	Counts
	APD Bias	APD Bias	Counts
	Range gate	Range gate	Adjusts T-0 mask
	PRF	PRF	See table AIV
	Failsafe	Failsafe	If start ignore, FAILSAFE = 1
	One stop	One stop	If cal ignore, ONE STOP = 1
	Auto acquire	Auto acquire	If auto acquire, Auto acquire = 1

given, one record per packet. There are 401 fields for each record (i.e., 400 data values per packet, plus the packet number) for either the normal or the high rate format FITS files. These are packet number, packet MET (which is the time of the first shot), and subprocess ID, comprising the first three fields; user data in the next 336 fields (for 56 shots in normal format or 112 shots in high rate format); and finally 62 fields for instrument status data from NLR packets and spacecraft housekeeping. These 62 fields include three data processing indices, NLR_DQI, CTP_DQI, SUB_DQI, which are used by the SDC and are not pertinent to data analysis. For all data values other than range and calibration, the conversions from counts to engineering units are given below.

TABLE AIa
Status 2, Science Packet Status Bits

Version 6	Version 7
Calibration counts of first shot	Minor frame of first shot
	Minor frame of second shot

In addition to data returned in science packets, instrument housekeeping information is returned in the spacecraft housekeeping data stream, some of which is commutated. The complete NLR housekeeping data sets are listed in Tables AIIa and AIIb. Noncommutated values are shown in Table AIIa as well as the times sampled for each of the subcommutation frames shown in Table AIIb. The subcommutated data values and the frames in which they appear are shown in Table AIIb. The names of the data values are listed in the first columns of Tables AIIa and AIIb and are given in the same order (top to bottom) as they appear in the NLR FITS files. Explanatory comments are always in the last column. In Table AIIb, the column labeled "Frame" gives the subcommutation frame in which the value is returned.

The op-codes corresponding to commands that appear among the status bits in the NLR packet data are listed in Table AIII. The hexadecimal op-codes are converted to decimal numbers in the NLR data sets.

The same information on PRF mode status is returned independently in both the NLR packet status bits (as "PRF") and the subcommutated housekeeping data (as "Pulse Repetition Frequency"), although the times of sampling are different. When PRF is returned as "2", NLR is firing at 1 Hz (see Table AIV).

Numerous quantities are returned in both the science packets and the housekeeping data, but are denoted by different names in the two data streams. The same scaling from counts to engineering units applies to both data streams, and the data are nearly always identical in the two cases; differences arise from the different sampling times. In what follows, if the same physical quantity is returned in both data streams with different names, both names are listed explicitly.

As noted in Table AI, the voltage threshold and calibration counts are returned for every shot in the normal science format. Moreover, the voltage threshold for one particular shot (which shot depending on DPU state, not determinate) is returned in the status bits. For the high rate format, the threshold (one shot, not determinate) and calibration values (last and first shots) are returned only in the status bits. In addition, the subcommutated housekeeping frame 3 contains one sample of calibration counts ("Fiber Optic Delay Assy Cal" which is offset by 256, see comment in Table AII) and one range sample ("Range Measurement"). Housekeeping subcommutation frame 2 contains one sample of threshold voltage ("Receiver Comparator Threshold"). As is conventional practice, all subcommutated housekeeping values are supplied for every record in the NLR FITS files, although only one frame is returned in any packet, by using the data sample nearest in time. Most housekeeping values are in any case slowly varying. The actual MET values for the individual subcommutation frames used to complete any record are given in the data words MET1 through MET5; these may or may not be exactly contemporaneous with the science user data in the record. In particular, the range value in the subcommutated housekeeping is at MET3.

To convert counts to the transmitter diode pump temperature in °C, the transmitter power supply temperature in °C, or the chassis deck temperature in °C,

$$T = 100 - \frac{155}{255} \times \text{counts}.$$

To convert counts to the time-of flight ASIC temperature in °C ("Time-of-Flight Temp" in NLR packet data), the receiver detector temperature in °C, or the medium voltage power converter temperature in °C,

$$T = \frac{84.668}{255} \times \text{counts} - 29.$$

To convert counts to receiver housing temperature in °C,

$$T = \frac{205}{255} \times \text{counts} - 100.$$

To convert counts to instrument main bus current in A ("Laser Rangefinder Current"),

$$I = \frac{0.8}{255} \times \text{counts}.$$

TABLE AIIa
NLR Housekeeping Data (Nonsubcommutated)

Nonsubcommutated values	Description	Comment
MET	Mission elapsed time	MET of housekeeping data
Laser rangefinder current	Laser rangefinder current	Counts
XMTR diode pump temp	Transmitter diode pump temp	Counts
XMTR power supply	Transmitter power supply temp	Counts
Chassis deck temp	Chassis deck temperature	Counts
Cover status	Cover status	Always equals 1
Rx housing	Receiver housing temperature	Counts
Cover release assy primary	Cover release assembly status	Always equals 0
Cover release assy secondary	Cover release assembly status	Always equals 0
Software version	DPU software version	Equals 6 or 7
Subcomm ID variable	Subcomm ID variable	Always equals 4
MET (first subcommutated frame)	MET (subcommutated frame 0)	Time of subcommutated data sample
MET (second subcommutated frame)	MET (subcommutated frame 1)	Time of subcommutated data sample
MET (third subcommutated frame)	MET (subcommutated frame 2)	Time of subcommutated data sample
MET (fourth subcommutated frame)	MET (subcommutated frame 3)	Time of subcommutated data sample
MET (fifth subcommutated frame)	MET (subcommutated frame 4)	Time of subcommutated data sample
Disaster code	Disaster code	Normally equals 0
MVPS voltage	MVPS voltage	Counts
APD bias voltage	APD bias voltage	Counts
DC/DC converter input current	DC/DC converter input current	Counts

Note. If entry in Comment field is "counts," the conversion to engineering units is given in the text of the Appendix.

TABLE AIIb
NLR Housekeeping Data (Subcommutated)

Subcommutated values	Frame	Comment
Command receive count	0	Count is modulo 16
Command reject count	0	Count is modulo 16
Failsafe mode	0	If FAILSAFE, =1
One stop signal mode	0	If ONE STOP, =1
Transmitter enable flag	0	If enabled, =1
Automatic acquisition mode	0	If Auto Acquire, =1
Range gate bits 6 to 3	0	Counts
Time of flight ASIC temperature	0	Counts
Receiver detector temperature	0	Counts
Memory dump address	1	Always equals 0
Memory dump data 1	1	Always equals 7
Memory dump data 2	1	Always equals 227
Power converter 15-V status	2	Normally equals 1
Power converter -15-V status	2	Normally equals 1
Power converter 5-V status	2	Normally equals 1
Power converter -5-V status	2	Normally equals 1
Power converter digital 5-V status	2	Normally equals 1
Housekeeping voltage subcom ID	2	0, 1, 2, 3, or 4; see Table AV
Power converter output	2	Counts
Receiver comparator threshold	2	Counts
Medium voltage power converter temperature	2	Counts
Fiber optic delay assy cal	3	Cal word of one shot (indeterminate), minus 256, expressed as unsigned integer
Spare	3	
Range measurement	3	Range word of one shot (indeterminate)
Pulse repetition frequency	4	See table AIV
Pulse count	4	Approx. count shot, modulo 16,777,216

Note. If entry in Comment field is "Counts," the conversion to engineering units is given in the Appendix.

TABLE AIII
NLR Command Op-codes

Command	Hexadecimal	Decimal
Shot rate	40	64
Fire Enable	41	65
Auto acquire	42	66
Calibrate	43	67
Set Threshold	45	69
Cal Ignore	46	70
Cal Restore	47	71
Start Ignore	48	72
Start Restore	49	73

TABLE AIV
Firing rate

PRF	Firing rate (Hz)
0	0
1	$\frac{1}{8}$
2	1
3	2
4	8

TABLE AV
Scaling Values for Subcommutated Power Converter Voltage

Name	Subcommutated ID	V_s (V)
DIG_5V	0	9.96
POS_5V	1	9.96
POS_15V	2	16.437
NEG_15V	3	−16.437
NEG_5V	4	−9.96

To convert counts to dc–dc converter input current in A,

$$I = \frac{0.996}{255} \times \text{counts}.$$

To convert counts to APD bias voltage in mV ("APD Bias" in NLR packets),

$$V = \frac{1073.12}{255} \times \text{counts}.$$

To convert counts to the medium voltage power supply voltage in V ("MVPS Voltage"),

$$V = \frac{747.94}{255} \times \text{counts}.$$

To convert counts to power converter output voltage in V,

$$V = \frac{V_s}{255} \times \text{counts},$$

where V_s is listed in Table AV.

To convert counts to threshold voltage in millivolts ("Threshold Voltage" in NLR packets, "Receiver Comparator Threshold" in housekeeping),

$$V = \frac{2307.1}{255} \times \text{counts}.$$

While the nominal values of the comparator threshold voltages are listed in Table I (for example., the threshold is 16 mV in TH = 0) the observed values of voltage counts at each value of TH are listed in Table AVI. The threshold in TH = 0 is actually set below the noise level in the receiver; this enables an in-flight measurement of the noise using the calibration pulse as discussed in the text. The threshold TH = 2 is far enough above the noise that the receiver false alarm rate (triggering on noise) is negligible. The threshold TH = 7 is high enough that the calibration pulse cannot be detected.

APPENDIX II—TEMPERATURE SENSITIVITY

During the Earth swingby test of January 19, 1998, the spacecraft was oriented such that NLR became directly illuminated by the Sun, and the NLR receiver housing was raised to ~10°C higher than maximum normal temperatures. At Eros, the spacecraft will always be oriented such that NLR is completely shadowed by the spacecraft, and such heating will not occur.

Figure A1 shows that even during the January 1998 Earth swingby test, the calibration counts measured by NLR in TH = 2 were unaffected (bottom), despite the temperature rise shown in the (top) panel. The lower panel of Fig. A1 plots the average of the calibration counts from the first shot and the last shot of every packet during the test. The temperature of the TOF ASIC (not shown) was constant to within 1 count (0.3°C) throughout the event. However, Fig. 5 shows that the average calibration counts measured in TH = 1 and 2 during this test (for all shots with valid calibrations) were about 0.4 counts lower than those measured 1 month earlier as well as lower than those measured subsequently. The significance of this difference is unclear. The conditions of the Earth swingby test have not been reproduced subsequently and will not occur at Eros. In summary, the in-flight calibration data provide no basis for introducing any temperature correction to measured ranges.

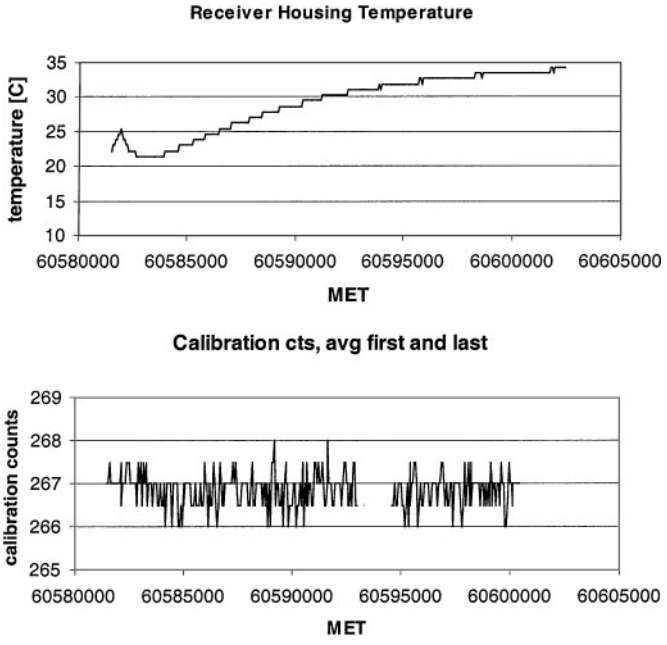

FIG. A1. Calibration counts versus instrument housing temprature, Earth swingby test.

TABLE AVI

Threshold Voltage Counts Observed In-Flight versus Commanded Threshold TH

TH	Threshold voltage counts
0	0, 1, 2
1	2, 3
2	6, 7
3	13, 14
4	27, 28, 29
5	53, 54, 55
6	113, 114, 115
7	224, 225, 226

ACKNOWLEDGMENT

This work was supported by NASA under the Near Earth Asteroid Rendezvous Project.

REFERENCES

Acuna, M., C. Russell, L. Zanetti, and B. Anderson 1997. The NEAR Magnetic Field Investigation: Science objectives at asteroid 433 Eros and experimental approach. *J. Geophys. Res.* **102**, 23751–23759.

Cheng, A. F., A. Santo, K. Heeres, J. Landshof, R. Farquhar, R. Gold, and S. Lee 1997. Near Earth Asteroid Rendezvous: Mission overview. *J. Geophys. Res.* **102**, 23695–23708.

Cole, T., M. Boies, A. El-Dinary, A. F. Cheng, M. Zuber, and D. E. Smith 1997. The Near Earth Asteroid Rendezvous laser altimeter. *Space Sci. Rev.* **82**, 217–253.

Gardner, C. S. 1992. Ranging performance of satellite laser altimeters. *IEEE Trans. Geosci. Remote Sens.* **30**, 5, 1061–1072.

Heeres, K., D. B. Holland, and A. F. Cheng 1997. The Near science data center. *Space Sci. Rev.* **82**, 283–308.

Izenberg, N., and B. Anderson 1998. NEAR Earth swings by Earthen route to Eros. *Eos Trans. AGU* **79**, 289.

Murchie, S. L., and C. Pieters 1996. Spectral properties and rotational spectral heterogeneity of 433 Eros. *J. Geophys. Res.* **101**, 2201–2214.

Rowlands, D. D., D. E. Pavlis, F. G. Lemoine, G. A. Neumann, and S. B. Luthcke 1999. The use of crossover constraint equations derived from laser altimetry in the orbit determination of Mars Global Surveyor. *Geophys. Res. Lett.* **26**, 1191–1194.

Smith, D. E., and 18 colleagues 1999. The global topography of Mars and implications for surface evolution. *Science* **284**, 1495–1503.

Trombka, J., and 12 colleagues 1997. Compositional mapping with the NEAR x-ray/gamma ray spectrometer. *J. Geophys. Res.* **102**, 23729–23750.

Veverka, J., and 12 colleagues 1997a. An overview of the NEAR multispectral imager-NEAR infrared spectrometer investigation. *J. Geophys. Res.* **102**, 23709–23727.

Veverka, J., and 16 colleagues 1997b. NEAR's flyby of 253 Mathilde: Images of a C-asteroid. *Science* **278**, 2109–2114.

Veverka, J., and 25 colleagues 1999. Imaging of asteroid 433 Eros during NEAR's flyby reconnaissance. *Science* **285**, 562–564.

Yeomans, D., A. Konopliv, and J.-P. Barriot 1997a. The NEAR radio science investigation. *J. Geophys. Res.* **102**, 23775–23780.

Yeomans, D., and 12 colleagues 1997b. Estimating the mass of asteroid 253 Mathilde from tracking data during the NEAR flyby. *Science* **278**, 2106–2109.

Yeomans, D., and 14 colleagues 1999. Estimating the mass of asteroid 433 Eros during the NEAR flyby. *Science* **285**, 560–561.

Yeomans, D. 1995. Asteroid 433 Eros: The target body of the NEAR mission. *J. Astronaut. Sci.* **43**, 417–426.

Zuber, M., D. E. Smith, A. F. Cheng, and T. D. Cole 1997. The NEAR laser ranging investigation. *J. Geophys. Res.* **102**, 23761–23773.

Zuber, M., D. E. Smith, F. Lemoine, and G. Neumann 1994. The shape and internal structure of the Moon from the Clementine mission. *Science* **266**, 1839–1843.

Zuber, M., D. E. Smith, S. Solomon, D. Muhleman, J. Head, J. Garvin, J. Abshire, and J. Bufton 1992. The Mars Observer laser altimeter investigation. *J. Geophys. Res.* **97**, 7781–7797.